PRELIMINARY NUMERICAL INVESTIGATION ON THE SEISMIC RESIDUAL CAPACITY OF REINFORCED CONCRETE PLASTIC HINGES

Alberto CUEVAS[1] Umut AKGUZEL[2] Joško OŽBOLT[3] and Stefano PAMPANIN[4]

ABSTRACT

This paper presents the results of experimental and numerical investigations on well-designed reinforced concrete beam-column joints. Nonlinear finite element (FE) analyses were performed, and experimental results of a two-thirds scale beam-column joint with the same characteristics subject to quasi-static displacement-controlled lateral loading were used to validate the numerical model. Subsequently, as part of a wider research project aiming at investigating the seismic residual capacity of reinforced concrete frames, parametric analyses under monotonic loading were performed targeting at investigating and understanding qualitatively and quantitatively the effect of parameters such as bond deterioration, steel and concrete material properties, as well as the amount of longitudinal reinforcement, on the cracking pattern and nonlinear behaviour of reinforced concrete plastic hinges.

INTRODUCTION

According to capacity design principles developed since the 1960s-1970s, structures are designed to withstand major earthquakes by developing inelastic action and energy dissipation in concentrated regions referred to as plastic hinges. This in turn, and almost inevitably when using traditional monolithic connections, leads to structural damage, often over the irreparability threshold. The aftermath of the Christchurch earthquakes sequence in 2010-2011 has highlighted the crucial need to move towards a damage control philosophy and low-damage technologies whilst improving assessment and repairing techniques for more traditionally designed plastic hinges (Pampanin, 2012).

Despite the availability and recent development of seismic assessment and rehabilitation guidelines, they are mainly focused to the evaluation of the vulnerability and improvement of the seismic performance of existing buildings designed prior to capacity design principles. Very little information and assistance is provided in assessing the residual capacity of damaged buildings, yet relatively well designed according to modern seismic codes, which leading to extensive post-earthquake demolitions due to the lack of knowledge on their residual capacity, in terms of number and intensity of aftershocks the structure could withstand following a major earthquake and during its remainder life-time. When considering the problem of residual capacity of typical plastic hinges, past research has tended to primarily focus on bridge columns (Kunnath et al., 1997; Mander and Cheng, 1999), and specifically on the assessment of the low-cycle fatigue of the longitudinal reinforcement (Mander et al., 1994; Abdalla et al., 2009; Haliweh et al., 2010), often based on the assumption that

---

[1] PhD Candidate, University of Canterbury, Christchurch, New Zealand, alberto.cuevasramirez@pg.canterbury.ac.nz

[2] PhD, Senior Structural Engineer, Beca Ltd, Christchurch, New Zealand, umut.akguzel@beca.com

[3] Professor, Institute for Construction Materials, University of Stuttgart, Germany, ozbolt@iwb.uni-stuttgart.de

[4] Professor, University of Canterbury, Christchurch, New Zealand, stefano.pampanin@canterbury.ac.nz

the failure in a reinforced concrete element can be attributed to either the low-cycle fatigue of the longitudinal reinforcing steel, the failure of the concrete due to either lack of confinement or the fracture of the transverse hoop reinforcement, and/or the buckling of the longitudinal reinforcement in compression. The latter two mechanisms can be easily avoided if sufficient transverse reinforcement is provided (Mander and Cheng, 1999). However, as it has been observed after recent earthquakes, the low cycle fatigue of the longitudinal reinforcement is only one part of the overall picture; there are other factors such as bond deterioration between steel and concrete, the amount of longitudinal and transverse reinforcement, as well as the characteristics of steel and concrete materials that strongly influences the plastic hinge behaviour, its cracking pattern and therefore, its overall residual capacity.

As part of a wider research project aiming at investigating the seismic residual capacity of reinforced concrete frames, this paper presents the results of an experimental and numerical investigation on a modern (i.e., relatively well-designed according to post-1970s seismic codes) reinforced concrete beam-to-column joint, targeting at identifying and understanding qualitatively and quantitatively the effect of parameters such as bond deterioration, steel and concrete material properties, as well as the amount of longitudinal reinforcement, on the cracking pattern and nonlinear behaviour of reinforced concrete plastic hinges. Figure 1 shows the key steps followed in the present study.

A well-designed according to NZS3101:2006 reinforced concrete beam-column joint is modelled by using the nonlinear finite element (FE) code MASA (Ožbolt et al., 2001). Experimental results of a beam-column joint with the same characteristics are used in order to validate the FE model and confirm its suitability to adequately represent the nonlinear behaviour of the beam-column joint. Subsequently, parametric analyses are performed in order to investigate the influence of various parameters on the cracking pattern in the plastic hinge region, at various limit states.
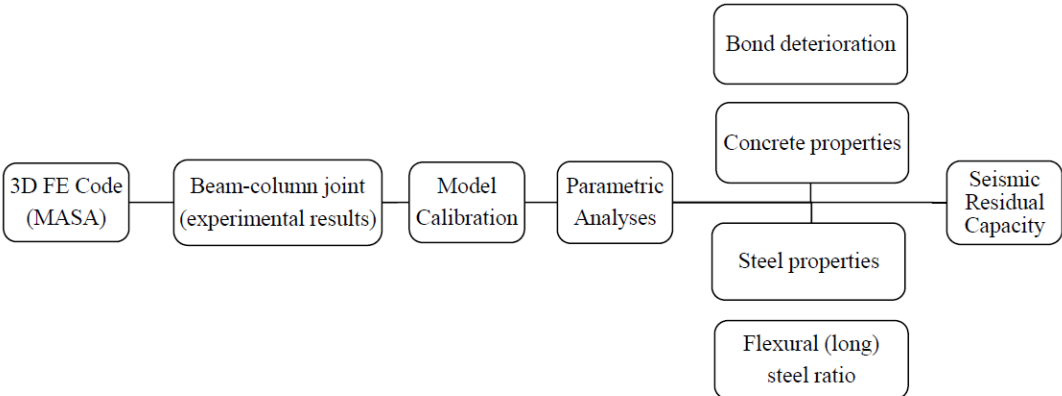
Figure 1. Overview of the research methodology followed in this study.

EXPERIMENTAL INVESTIGATION

As previously anticipated, prior to perform parametric analyses the FE model has been validated with the experimental results of a beam-column joint designed according to the latest concrete code in NZ (NZS3101:2006, under review and amendments following the 2010-2011 earthquakes sequence) to achieve a weak-beam and strong-column hierarchy.

Specimen description

The test specimen is a two-thirds scale, two-dimensional exterior reinforced concrete beam-column joint (see Figure 2). The beam is 255mm wide by 325mm high with 4-D12 deformed longitudinal bars (top and bottom) and plain D6 bars as transverse reinforcement. The column is 255mm by 255mm with 12-D12 deformed longitudinal bars and plain D6 bars as transverse reinforcement. Following capacity design principles, the column was designed to remain elastic throughout the experimental test by allowing the yield moment capacity of the column to be well

above the yield moment capacity of the beam. The plastic hinge region as well as the joint is detailed with two stirrups (one internal and one external) in order to prevent a brittle shear failure.
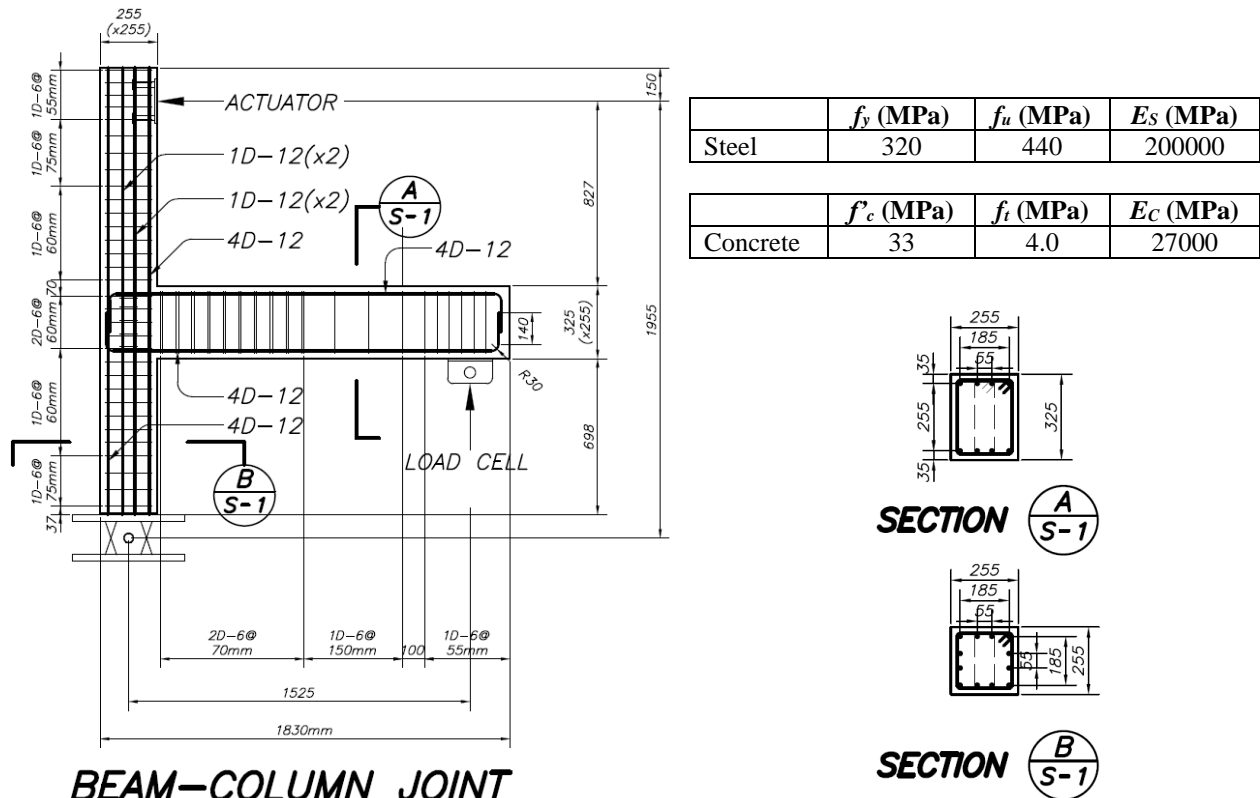

	f_y (MPa)	f_u (MPa)	E_S (MPa)
Steel	320	440	200000

	f'_c (MPa)	f_t (MPa)	E_C (MPa)
Concrete	33	4.0	27000

Figure 2. Experimental setup of the two-thirds scale specimen and material characteristics.

Experimental program and testing procedure

As shown in Figure 2, the column was pinned at the base to represent the point of contra-flexure at mid-height of the column, whereas the beam was vertically supported by a load cell restraining the vertical direction and allowing lateral movement (i.e., simulating a roller support at mid-span of the beam length). A constant axial force of 65kN, representing the gravity loads, was applied at the top of the column, and a quasi-static displacement-controlled cycling loading protocol was applied at the top of the column (increasing top drifts of ±0.1%, ±0.2%, ±0.35%, ±0.5%, ±0.75%, ±1.0%, 1.5%, ±2.0%, ±2.5%, ±3.5%, and ±4.5%, see Figure 3) as per the acceptance criteria of the American Concrete Institute for moment frames (ACI, 2001).
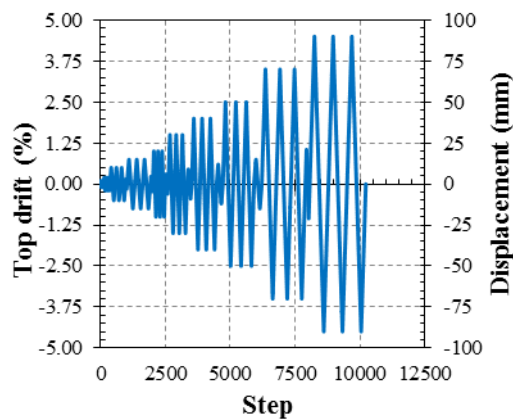

Figure 3. Schematic representation of the applied loading protocol.

NUMERICAL INVESTIGATION

Finite element numerical model

The nonlinear FE code MASA developed at the Institute for Construction Materials (IWB) of the University of Stuttgart (Ožbolt et al., 2001), was used in this study. In this code the concrete is modelled according to a microplane model, consisting of a three-dimensional (3D) microscopic model in which the material is characterized by uniaxial relations between the stress and strain components on planes of various orientations called "microplanes". The smeared-crack concept was used for the modelling of the cracking of the concrete, and the reinforcing bars were represented with one-dimensional (1D) truss elements with a three-linear constitutive law.

The bond between the longitudinal reinforcement and concrete was modelled using discrete bond elements consisting of 1D nonlinear springs (see Figure 4), whereas for transverse reinforcement a rigid connection between steel and concrete was assumed, neglecting the influence of the relative displacement between the stirrups and the concrete (Eligehausen et al., 2009). This discrete bond model is able to predict the bond behaviour of deformed bars under monotonic and cyclic loading; the bond deterioration is assumed to occur after some slip due to mechanical damage in the concrete-to-steel interface surrounding the ribs (Eligehausen et al., 1983; Lettow, 2006).

Hexahedral elements with side lengths of approximately 15mm in the joint area and the plastic hinge regions, as well as 50mm elsewhere were used to create the mesh of the elements. Linear elastic elements were used at the vicinities of the supports and the point of load application so that local failure of concrete elements due to excessive stresses is avoided. Mirror symmetry (i.e., symmetry about a vertical plane across a mid-section in the beam-column joint) was used to drastically reduce the total amount of nodes and elements and thus the required computational time.

The material properties used in the simulations are listed in Table 2. BCJ-1 refers to the original (i.e., experimentally tested) beam-column joint; whereas BCJ-2 to BCJ-12 are further used for parametric analyses under monotonic loading. It is important to mention that parametric analyses under cyclic loading are currently under development and will follow as part of the overall project.
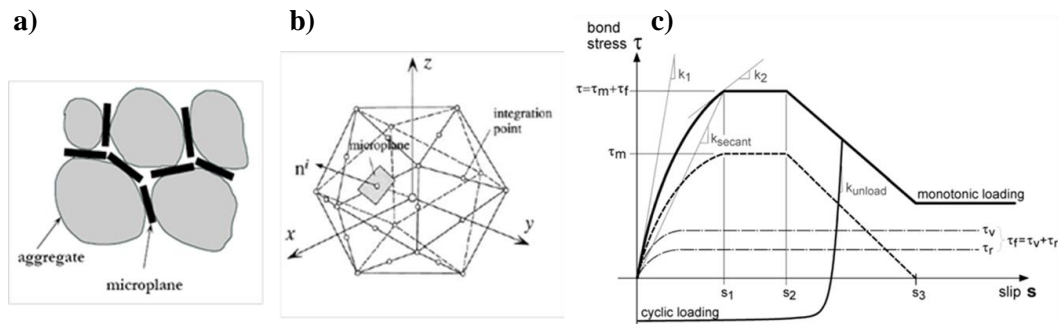

Figure 4. Microplane model: a) load transfer over a number of idealized contact planes; b) spatial discretization of unit-volume sphere by 21 microplanes (Ozbolt et al., 2001); c) Discrete bond model as implemented in MASA (Lettow, 2006).

NUMERICAL- EXPERIMENTAL COMPARISON

Figure 5a shows the cyclic lateral force-displacement response from the quasi-static test. The hysteresis loops show a fat and fairly stable shape with some minor pinching, which might be attributed to the opening and closing of cracks as well as some level of bond degradation. In the same figure the monotonic curve obtained from numerical analysis is shown; the agreement between this curve and the envelope of the cyclic response is evident. Figure 5b shows the same monotonic curve with indications for different limit states. For normal structures, Level 1 (Serviceability Limit State, SLS) refers to a 50% probability of exceedance in 50 years intensity level; Level 2 (Damage-control Limit State, DLS) to a 10% probability of exceedance in 50 years intensity level; and Level 3

(Ultimate Limit State, ULS) to a 2% probability of exceedance in 50 years. The strain limits proposed in Priestley et al. (2007) and listed in Table 1 were adopted in this study.

Table 1. Strain limits for different design intensity levels (Priestley et al., 2007)

| Material	Level 1 (SLS)	Level 2 (DLS)	Level 3 (ULS)
Concrete compressive strain	0.004	$\varepsilon_{cu} < 0.02$	1.5 ε_{cu}
Rebar tension strain	0.015	$0.60\varepsilon_{su} < 0.05$	$0.90\varepsilon_{su} < 0.08$

In the previous table,

$$\varepsilon_{cu} = 0.004 + \frac{1.4 \cdot \rho_s \cdot f_{yh} \cdot \varepsilon_{su}}{f'_{cc}} \tag{1}$$

$$f'_{cc} = f'_c \cdot \left\{ 2.254 \cdot \sqrt{1 + \frac{7.94 \cdot f_l}{f'_c}} - 2 \cdot \frac{f_l}{f'_c} - 1.254 \right\} \tag{2}$$

$$f_l = 0.50 \cdot C_e \cdot \rho_v \cdot f_{yh} \tag{3}$$

$$\rho_v = \rho_{ax} + \rho_{ay} \tag{4}$$

where ε_{cu} is the ultimate compression strain for confined concrete; f'_{cc} is the compression strength of the confined concrete, in MPa; f'_c is the unconfined compression concrete strength, in MPa; f_l is the lateral confining stress, in MPa; ρ_v is the volumetric confinement ratio; ρ_{ax} and ρ_{ay} are the area ratio of transverse reinforcement in the x and y direction, respectively; and ε_{su} is the ultimate strain for the longitudinal reinforcement, assumed to be 0.015.
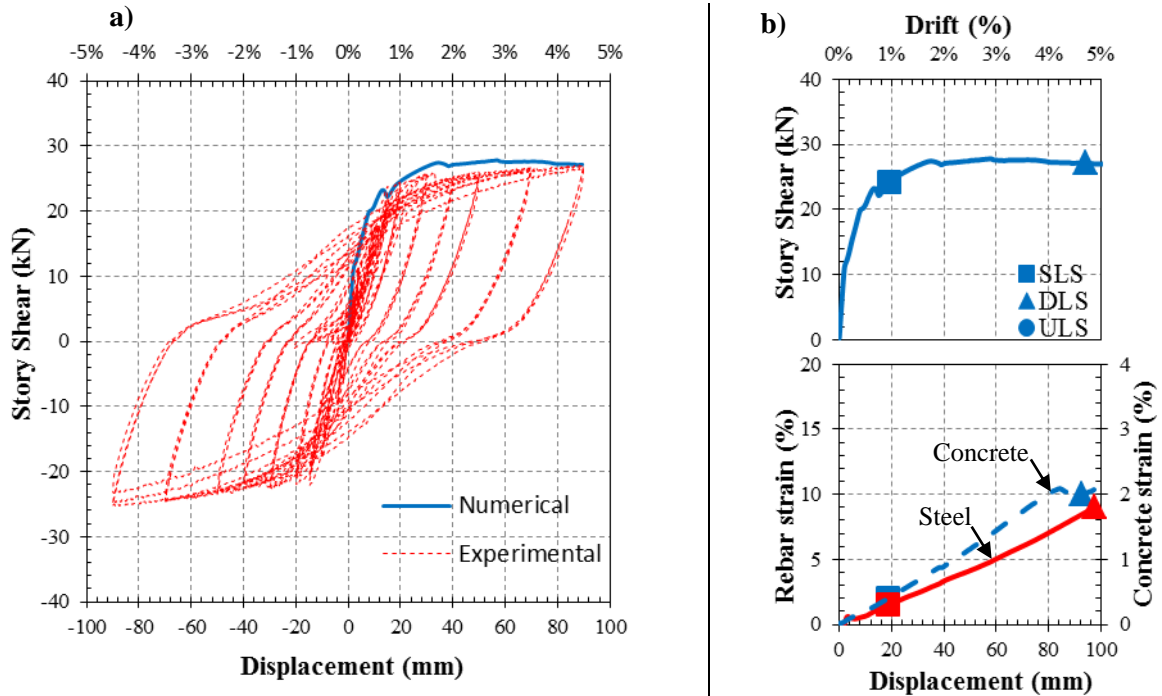
Figure 5. (a) Cyclic and monotonic lateral force displacement response from the experimental (dotted line) and numerical (solid line) results (BCJ-1), respectively; (b) Monotonic curve from the numerical simulation (BCJ-1, top); and steel and concrete strains (bottom) from the numerical simulation (the dashed-line represents concrete strain, whereas the solid line represent the rebar strain). The solid square represents the Serviceability Limit State (SLS); the solid triangle the Damage-control Limit State (DLS); and the solid circle the Ultimate Limit State (ULS, not observed here since it occurs at higher drift levels).

Figure 5b also shows the strains measured at the bottom steel rebars and top concrete fibre of the plastic hinge obtained from the FE model. It is evident how they follow a fairly linear trend increasing in proportion to the applied lateral displacement. It is interesting to note that both the SLS and DLS strain limits occur almost simultaneusly at the steel and concrete fibres, at 0.95% and ~4.7% drift angles, respectively.

Figure 6 shows snapshots of the crack patterns in the specimen during the experimental campaign at drifts angles of 1.0%, 1.5%, 2.0%, 2.5%, 3.5%, and 4.5%. Several minor cracks and one-to-two major cracks form and propagate through the beam height as the drift angle increases. At the end of the experimental test (i.e., at 4.5% drift angle), two major cracks and concrete crushing at the plastic hinge zone along with minor cracking at the beam-column joint and their surroundings are apparent.

Figure 6 shows also the expected cracking pattern obtained from the FEM model under monotonic loading. As seen in this figure, the two major cracks as well as the minor cracks at the joint area observed during the experimental test are well simulated by the numerical model.
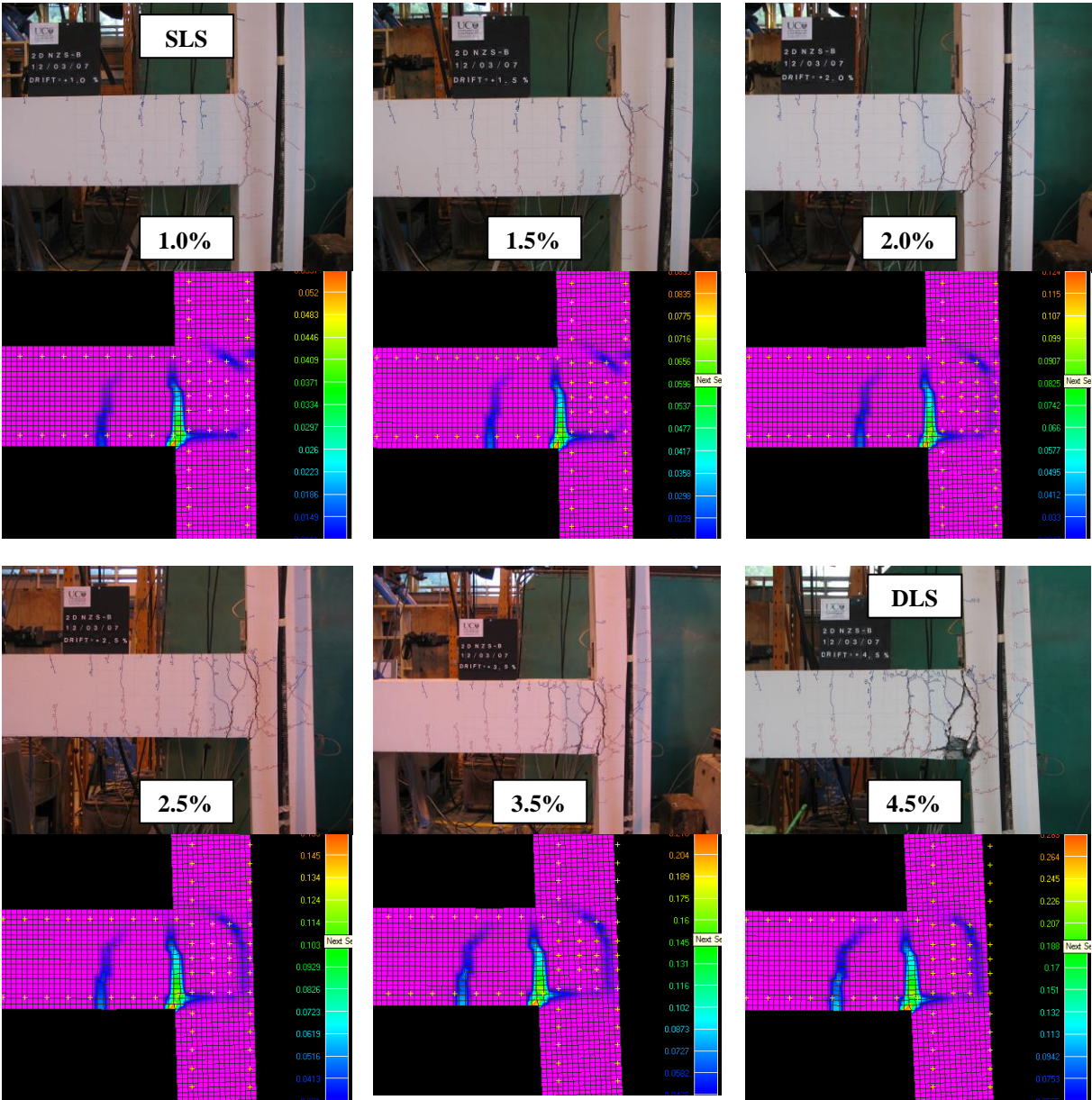

Figure 6. Snapshots showing the cracking pattern at drift angles of 1.0%, 1.5%, 2.0%, 2.5%, 3.5% and 4.5%. The figure below each snapshot represents the corresponding cracking pattern obtained with the FE modeling (i.e., monotonic loading BCJ-1).

One intriguing aspect of this experimental and numerical campaign is the formation of two major cracks in the plastic hinge region of a well-designed and detailed beam-column joint. Interestingly enough, this peculiarity agrees very well with observations following the 2010-2011 Canterbury earthquake sequence, where in a number of cases few major crack openings were observed instead of a well distributed cracking pattern expected in those plastic hinge locations were plastic deformation was expected to occur. The small number of cracks induces a large amount of deformation concentrated at a single location, which might lead to a low-cycle fatigue of the reinforcing steel. This effect may be attributed to low reinforcement ratios, low-rate of strain-hardening of the steel and/or high concrete tensile strengths, as well as high loading speed (SESOC, 2011, see also Kam et al., 2011).

In the present case, the longitudinal reinforcement ratio ρ_s of 0.61% (very close to the lower bound limit ρ_{min} of 0.45% as per NZS3101:2006), as well as the tensile concrete strength f_t of 4MPa (close enough to an expected upper bound limit of 5MPa) second the above statement.

PARAMETRIC ANALYSES, MONOTONIC LOADING

The objective of the parametric analyses was to identify the most critical parameters (see Figure 1) and combinations of them that affect the cracking pattern and the residual capacity of typical plastic hinges. This information will be later used as part of a wider research project to calibrate the damage observed in real structures after recent earthquakes, with the aim of developing analytical models capable of modelling the residual capacities of plastic hinges to be used for either a pre or post-earthquake assessment of existing buildings as well as seismic design of new ones (see Cuevas and Pampanin, 2014, for further details).

Table 2 lists the different range of values for each parameter assumed during the parametric analyses. As previously mentioned the model BCJ-1 was used as the benchmark, and each series of the tabulated values was then modified accordingly. The bond characteristics were computed as suggested by Lettow (2007), with a difference s_2-s_1 (length of the slipping plateau see Figure 4c) fixed at 0.80mm, and s_3, the slip at which mechanical bond resistance is lost, assumed to be 8.5mm and 10mm for D12 and D16 bars, respectively (Christoph, 2012).

Table 2. Material and bond characteristics used for numerical simulation and parametric analyses (the bond parameters are schematically defined in Figure 4c).

	BCJ-1	BCJ-2	BCJ-3	BCJ-4	BCJ-5	BCJ-6	BCJ-7	BCJ-8	BCJ-9	BCJ-10	BCJ-11	BCJ-12
f'_c (MPa)	33	20	20	20	20	40	40	40	40	33	33	33
f_t (MPa)	4.00	3.58	3.58	3.58	3.58	5.06	5.06	5.06	5.06	2.00	3.50	5.00
E_c (MPa)	26983	21750	21750	21750	21750	27900	27900	27900	27900	26983	26983	26983
f_y (MPa)	320	300	300	500	500	300	300	500	500	320	320	320
f_u (MPa)	440	412.5	412.5	687.5	687.5	412.5	412.5	687.5	687.5	440	440	440
ρ_s (%)	0.61	0.61	1.09	0.61	1.09	0.61	1.09	0.61	1.09	0.61	0.61	0.61
$\tau = \tau_m + \tau_f$ (MPa)	13.7	10.7	11.9	10.7	11.9	15.1	16.8	15.1	16.8	13.7	13.7	13.7
τ_m (MPa)	8.21	6.39	7.11	6.39	7.11	9.04	10.06	9.04	10.06	8.21	8.21	8.21
k_1 (MPa/mm)	35.2	28.6	34.1	28.6	34.1	38.7	45.1	38.7	45.1	35.2	35.2	35.2
k_2 (MPa/mm)	1.28	1.04	0.85	1.04	0.85	1.41	1.13	1.41	1.13	1.28	1.28	1.28
k_{sec} (MPa/mm)	16.0	13.0	14.2	13.0	14.2	17.6	18.8	17.6	18.8	16.0	16.0	16.0
s_1 (mm)	0.86	0.82	0.84	0.82	0.84	0.86	0.89	0.86	0.89	0.86	0.86	0.86

Influence of concrete and steel strength, f'_c, f_y, and longitudinal reinforcement ratio, ρ_s:

Figure 7 shows the results of numerical simulations with unconfined compressive concrete strength f'_c of 20MPa, with longitudinal reinforcement ratio ρ_s of 0.61% (BCJ-2 and BCJ-4) and 1.09% (BCJ-3 and BCJ-5, respectively). BCJ-2 and BCJ-3 have a yield strength f_y of 300MPa, whereas BCJ-4 and BCJ-5 of 500MPa. The nonlinear behaviour of BCJ-2 is similar to BCJ-1, although its reduction in shear capacity is coupled with a reduction in the expected level of damage (see Figure 7a, e). Furthermore, although the plastic hinges of BCJ-3 and BCJ-4 have comparable yield moment capacities (in terms of area of steel times nominal yield strength), there are significant

differences in the nonlinear behaviour; while BCJ-3 has a peak shear capacity at SLS and then drops abruptly (see Figure 7f); the nonlinear behaviour of BCJ-4 is more uniform with a strength drop at higher drift angles ~3% (see Figure 7g). Nevertheless, the expected cracking pattern is comparable in both cases with joints severely damaged at drift angles close to the ULS. BCJ-5 behaves in a similar fashion as BCJ-3, although more damage in the joint is expected due to a higher shear demand at higher drifts (see Figure 7h).
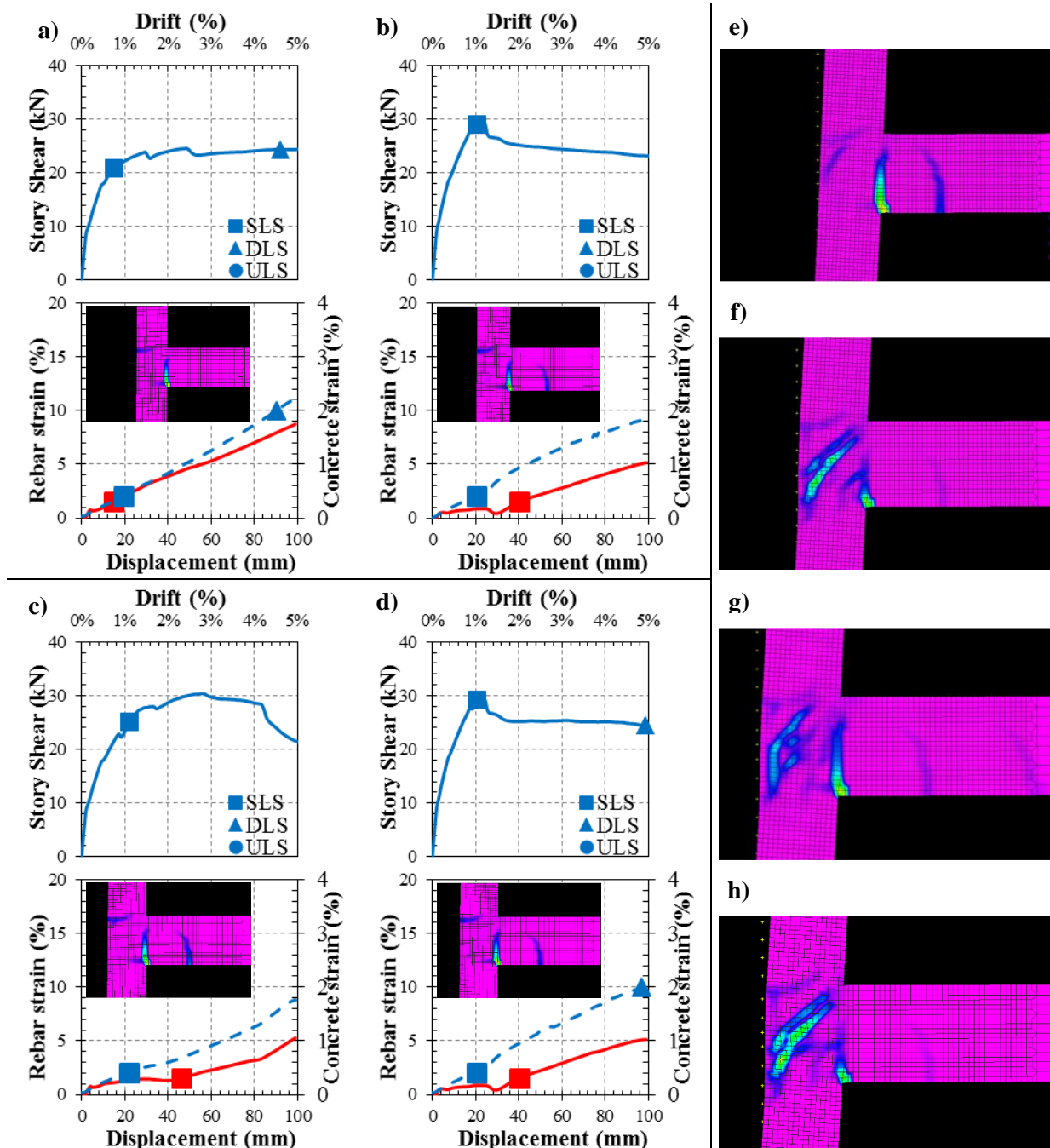

Figure 7. Monotonic story shear vs displacement response from the numerical results; and steel and concrete strains for simulations: a) BCJ-2; b) BCJ-3; c) BCJ-4; and d) BCJ-5 (the dashed-line represents concrete strains, whereas the solid line represent the rebar strain; the small snapshot represent the cracking pattern at SLS). Snapshots for e) BCJ-2 at DLS; f) BCJ-3 at drift equivalent to DLS of BCJ-2; g) BCJ-4 at drift equivalent to DLS of BCJ-4; and h) BCJ-5 at DLS. The solid square represents the Serviceability Limit State (SLS); the solid triangle the Damage-control Limit State (DLS); and the solid circle the Ultimate Limit State (ULS, not observed here).

Figure 8 shows the results of numerical simulations with unconfined compressive concrete strength f'_c of 40MPa, with longitudinal reinforcement ratio ρ_s of 0.61% (BCJ-6 and BCJ-8) and 1.09% (BCJ-7 and BCJ-9, respectively). BCJ-6 and BCJ-7 have a yield strength f_y of 300MPa, whereas BCJ-8 and BCJ-9 of 500MPa. The nonlinear behaviour of BCJ-6 is similar to BCJ-1, although a single major crack opening instead of two major cracks is expected to occur (see Figure 8a, e).
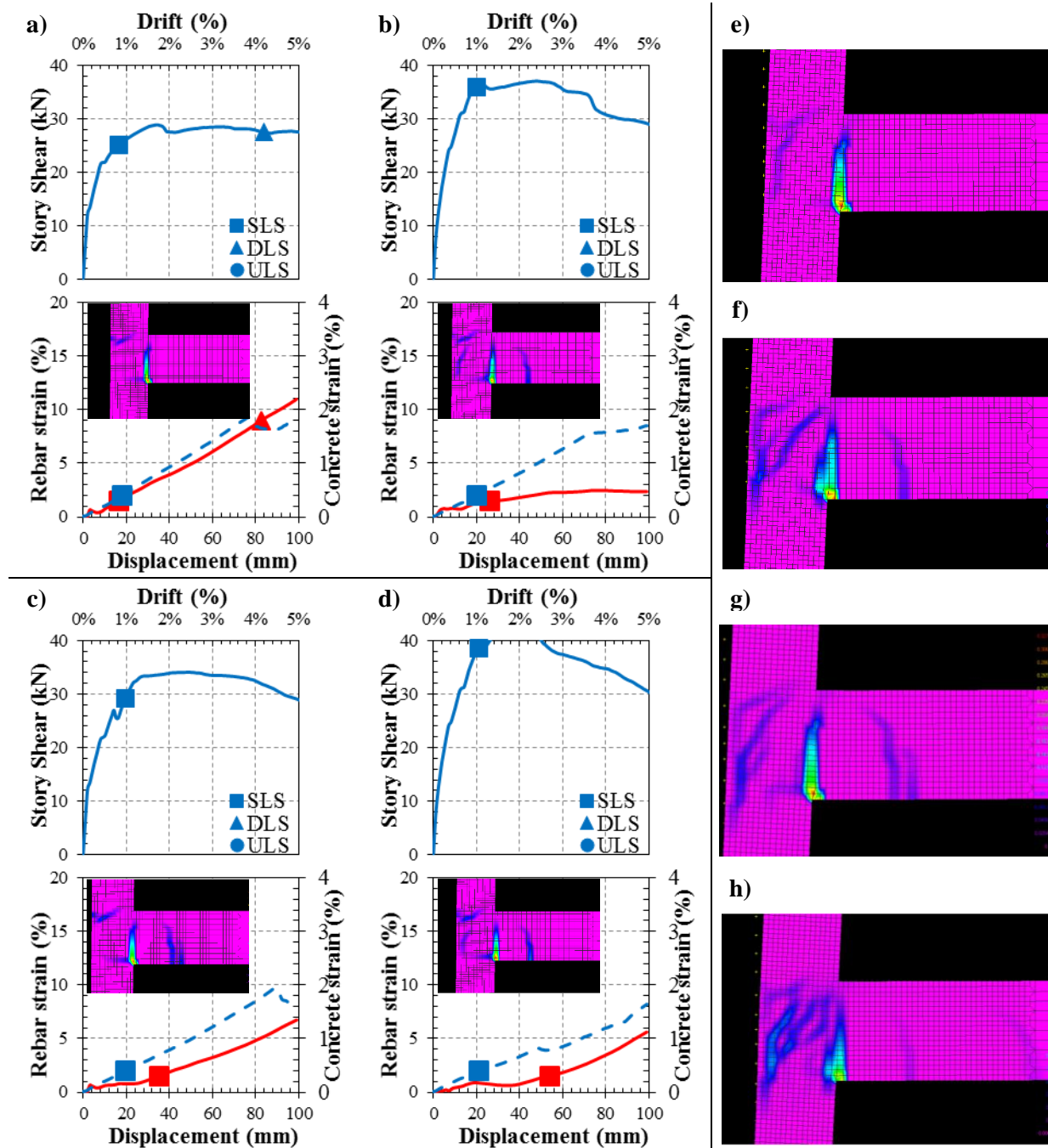

Figure 8. Monotonic story shear vs displacement response from the numerical results; and steel and concrete strains for simulations: a) BCJ-6; b) BCJ-7; c) BCJ-8; and d) BCJ-9 (the dashed-line represents concrete strains, whereas the solid line represent the rebar strain; the small snapshot represent the cracking pattern at SLS). Snapshots for e) BCJ-6 at DLS; f) BCJ-7 at drift equivalent to DLS of BCJ-6; g) BCJ-8 at 4.5% drift; and h) BCJ-9 at 4.5% drift. The solid square represents the Serviceability Limit State (SLS); the solid triangle the Damage-control Limit State (DLS); and the solid circle the Ultimate Limit State (ULS, not observed here).

Furthermore, although the plastic hinges of BCJ-7 and BCJ-8 have comparable yield moment capacities (in terms of area of steel times nominal yield strength), their nonlinear behaviour and cracking pattern show significant differences; less and major cracks are expected to occur for smaller f_y and larger ρ_s (i.e., BCJ-7). BCJ-9 behaves in a similar fashion as BCJ-3 and BCJ-5, although more shear capacity strength drop is expected to occur (see Figure 8h).

By comparing Figure 7 and Figure 8, it is evident how f'_c affects the cracking level at the joint. Furthermore, it is interesting to note how the residual shear strength of the beam-column joints is influenced also by f'_c irrespective of f_y and ρ_s, being on average 23kN and 30kN for f'_c of 20MPa and 30MPa, respectively. Therefore, the increased level of damage observed in Figure 7 with respect to Figure 8 can be attributed to a reduced shear capacity due to a low compressive strength. In addition, the previous figures show drifts at SLS fairly constant irrespective of f'_c, f_y and ρ_s (1.0% on average, except for BCJ-2 and BCJ-6 where values around 0.8% were obtained). The above might be explained with the fact that the yield curvature is relatively insensitive to the axial load and reinforcement ratio, depending mainly on structural geometry and material sizes (Priestley et al., 2007).

Influence of f_t on the cracking pattern and limit states:

In the previous figures it was observed that variations on f'_c affect the expected cracking pattern in the beam-column joints. Since the unconfined compressive concrete strength has a strong impact on the tensile concrete strength, three additional simulations with f_t of 2MPa (BCJ-10), 3.5MPa (BCJ-11) and 5MPa (BCJ-12), representing realistic values for f'_c of 30-to-35MPa, were adopted by keeping unchanged the other parameters. In Figure 9, although the overall behaviour of the three simulations is comparable in terms of strength, stiffness and strain limits, the cracking pattern is strongly affected by the tensile strength of concrete f_t, being more uniform (i.e., larger amount and less intense cracks) for lower values, and more concentrated in one single crack for higher values. This latter behaviour is consistent with the observations occurred in the aftermath of the Canterbury earthquakes sequence and confirms the primary role that the tensile strength of concrete, for other constant parameters, can have in the cracking pattern and thus residual capacity of structural components and connections.
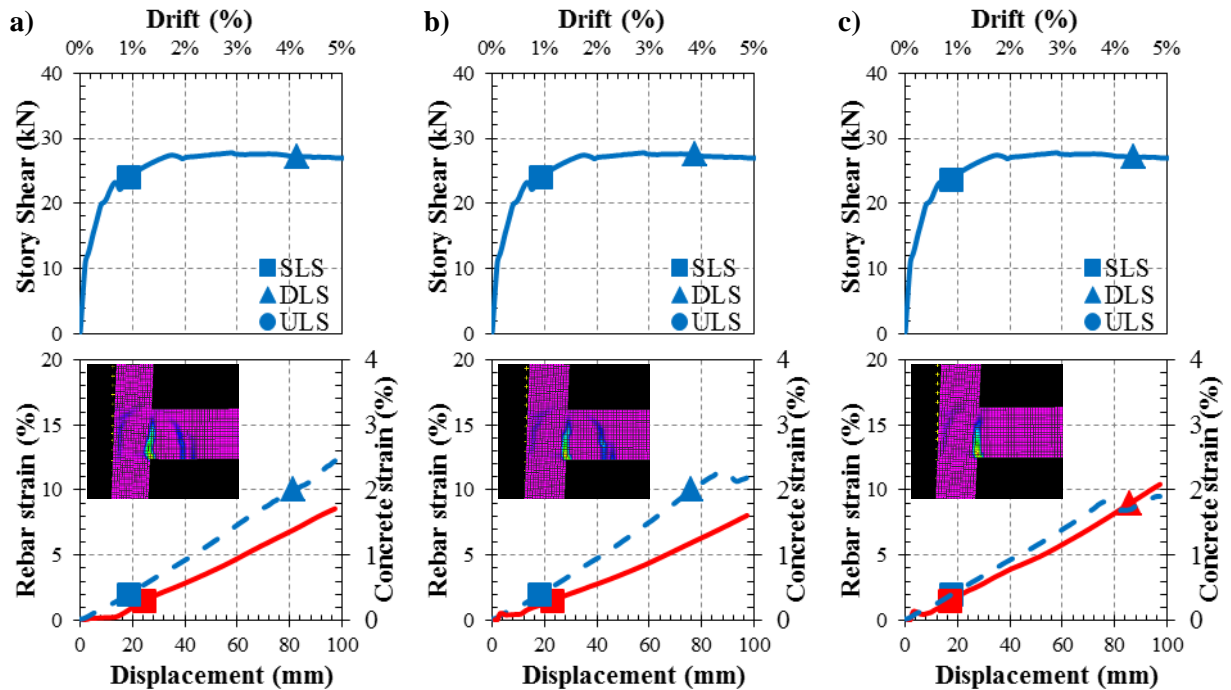

Figure 9. Monotonic story shear vs displacement response from the numerical results; and steel and concrete strains for simulations: a) BCJ-10; b) BCJ-11; c) BCJ-12 (the dashed-line represents concrete strains, whereas the solid line represent the rebar strain; the small snapshot represent the cracking pattern at DLS). The solid square represents the Serviceability Limit State (SLS); the solid triangle the Damage-control Limit State (DLS); and the solid circle the Ultimate Limit State (ULS, not observed here).

CONCLUSIONS

This paper presents the results of experimental and numerical investigations on well-designed reinforced concrete beam-to-column joints, targeting at identifying and understanding qualitatively and quantitatively the effect of parameters such as bond deterioration, steel and concrete material properties, as well as the amount of longitudinal reinforcement, on the cracking pattern and nonlinear behaviour of reinforced concrete plastic hinges. This study is part of a wider research project aiming at investigating the seismic residual capacity of reinforced concrete frames. The information contained herein will be later used to calibrate the damage observed in real structures after recent earthquakes, with the aim of developing analytical models capable of modelling the residual capacities of plastic hinges to be used for seismic design as well as either a pre or post-earthquake assessment of existing buildings.

Two major cracks in the plastic hinge region were observed during the numerical simulation and experimental validation, which agrees well with observations following the 2010-2011 Canterbury earthquake sequence, where in a number of cases few major crack openings were observed instead of a well distributed cracking pattern expected in those plastic hinge locations, condition attributed to either a low-rate of strain-hardening of the steel, low reinforcement ratio, high loading speed, and high concrete tensile strengths as in the present case. The negative aspect of the small number of cracks in a plastic hinge is mainly the large amount of deformation induced at a single location, leading a low-cycle fatigue of the reinforcing steel and consequently, of the whole plastic hinge region.

Parametric analyses under monotonic loading have shown that less amount and major crack openings are expected to occur for smaller f_y and larger ρ_s values. Moreover, it was observed that although the overall behaviour in terms of strength, stiffness and strain limits is not significantly affected by variations in f_t, it strongly affects the expected cracking pattern in the beam-column joints, the latter being more uniform (i.e., larger amount and less intense cracks) for lower f_t values. Furthermore, the seismic residual shear strength of the beam-column joints was observed to be influenced also by f'_c irrespective of the f_y and ρ_s values. Parametric analyses under cyclic loading is under development and will follow as part of the overall project.

REFERENCES

Abdalla, J. A., Hawileh, R. A., Abdelrahman, K. (2009) "Energy-based prediction of low-cycle fatigue life of BS 460B and BS B500B steel bars," Materials and Design, 30:4405-4413.

ACI. (2001). "Acceptance Criteria for Moment Frames Based on Structural Testing (T1.1-01) and Commentary (T1.1R-01)," A. I. T. G. 1, ed., Farmington Hills, Michigan.

Cuevas, A., Pampanin, S. (2014) "Accounting for residual capacity of reinforced concrete plastic hinges: current practice and proposed framework," 2014 New Zealand Society of Earthquake Engineering Conference, Auckland, New Zealand.

Eligehausen, R., Genesio, G., Ozbolt, J., Pampanin, S. (2009) "3D analysis of seismic response of RC beam-column exterior joints before and after retrofit," Concrete Repair, Rehabilitation and Retrofitting II, 1141-1147.

Hawileh, R., Rahman, A., Tabatabai, H. (2010) "Evaluation of the low-cycle fatigue life in ASTM A706 and A615 grade 60 steel reinforcing bars," Journal of Materials in Civil Engineering, 22(1):65-76.

Kam, W. Y., Pampanin, S., Elwood, K. (2011) "Seismic performance of reinforced concrete buildings in the 22 February Christchurch (Lyttelton) Earthquake," Bulletin of the New Zealand Society for Earthquake Engineering, 44(4):239-278.

Kunnath, S. K., El-Bahy, A., Taylor, A. W., Stone, W. C. (1997) "Cumulative seismic damage of reinforced concrete bridge piers," National Institute of Standards and technology, Technical Report NISTIR-6075.

Lettow, S. (2006) "Ein Verbundelement für nichtlineare Finite Elemente Analysen – Anwendung auf Übergreifungsstöße (A bond element for nonlinear finite element analysis – Applied on splices)," PhD Dissertation, IWB, Universität Stuttgart, Germany (in German).

Mahrenholtz, C (2012) "Seismic bond model for concrete reinforcement and the application to column-to-foundation connections," PhD thesis, Institut fur Werkstoffe im Bauwesen der Universitat Stuttgart.

Mander, J. B., Cheng, C. T. (1999) "Replaceable hinge detailing for bridge columns," SP-187 Seismic Response of Concrete Bridges, ACI Symposium Publications.

Mander, J. B., Panthaki, F. D., Kasalanati, A. (1994) "Low-cycle fatigue behaviour of reinforcing steel," Journal of Materials in Civil Engineering, 6(4):453-468.

Ožbolt J, Yijun L, Kozar I. (2001) "Microplane model for concrete with relaxed kinematic constraint," International Journal of Solids and Structures. 2001, 38:2638-711.

Pampanin, S. (2012) "Reality-check and renewed challenges in earthquake engineering: implementing low-damage structural systems – from theory to practice," Fifteenth World Conference in Earthquake Engineering, Lisbon, Portugal.

Priestley, M. J. N., Calvi, G. M, Kowalski, M. J. (2007) Displacement-based seismic design of structures, IUSS Press, Pavia, Italy.

SESOC (2011) "Preliminary observations from Christchurch earthquakes" Structural Engineering Society, New Zealand.